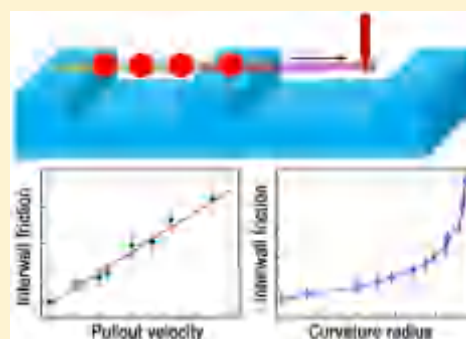


Interwall Friction and Sliding Behavior of Centimeters Long Double-Walled Carbon Nanotubes

Rufan Zhang,[†] Zhiyuan Ning,[‡] Ziwei Xu,[§] Yingying Zhang,^{*,‡} Huanhuan Xie,^{†,‡} Feng Ding,[§] Qing Chen,[†] Qiang Zhang,[†] Weizhong Qian,[†] Yi Cui,^{¶,||} and Fei Wei^{*,†}[†]Beijing Key Laboratory of Green Chemical Reaction Engineering and Technology, Department of Chemical Engineering, Tsinghua University, Beijing 100084, China[‡]Key Laboratory for the Physics and Chemistry of Nanodevices, Peking University, Beijing 100871, China[§]Institute of Textiles and Clothing, Hong Kong Polytechnic University, Kowloon, Hong Kong 999077, China[‡]Department of Chemistry and Center for Nano and Micro Mechanics, Tsinghua University, Beijing 100084, China[¶]Department of Materials Science and Engineering, Stanford University, Stanford, California 94305, United States^{||}Stanford Institute for Materials and Energy Sciences, SLAC National Accelerator Laboratory, 2575 Sand Hill Road, Menlo Park, California 94025, United States

* Supporting Information

ABSTRACT: Here, we studied the interwall friction and sliding behaviors of double-walled carbon nanotubes (DWCNTs). The interwall friction shows a linear dependence on the pullout velocity of the inner wall. The axial curvature in DWCNTs causes the significant increase of the interwall friction. The axial curvature also affects the sliding behavior of the inner wall. Compared with the axial curvature, the opening ends of DWCNTs play tiny roles in their interwall friction.



KEYWORDS: Carbon nanotubes, superlubricity, friction, interaction, ultralong curvature

Micro/nano-electrical-mechanical systems (M/NEMS) have been witnessed with flourishing development in the past decades, in company with new scientific studies and technical applications.¹ With the reduction of mass and volume, the interfacial friction becomes a bottleneck for M/NEMS due to their extremely high surface-to-volume ratio.^{2,3} Despite the fundamental and practical importance of friction and the growing efforts in the field, many key aspects of this phenomenon are still not well understood. Extensive studies have been focused on reducing frictions between solid surfaces, and a new concept, superlubricity (a phenomenon in which friction almost vanishes between two incommensurate solid surfaces),^{4–12} was proposed. It is always a challenge to study friction at the nano- or even atomic scale. Multiwalled carbon nanotubes (MWCNTs), consisting of multiple coaxial cylindrical walls with an approximate wall spacing of 0.34 nm and extremely high aspect ratios (10^3 – 10^8), are known with only van der Waals (vdW) interaction rather than chemical bonds between their walls.^{13–18} The inner walls of MWCNTs tend to slide or rotate easily against the outer ones under external loadings, rendering them an ideal candidate for the study of interfacial friction and superlubricity ranging from nano- to macroscale and for the fabrication of M/NEMS such as

ultrahigh frequency longitudinal oscillators, nanomotors, fast switches, ultrasensitive sensors, fine positioning devices, gyroscopes, etc.

Because of the difficulty in nanomanipulation, only a few experimental studies were reported on the sliding or rotational behaviors of MWCNT walls^{19–24} in spite of the progress in the theoretical studies on the interwall interactions of MWCNTs.^{13–16,18,25–28} For example, a “sword-in-sheath” mechanism was proposed to interpret the sliding of inner walls in MWCNTs.²³ A controlled and reversible telescopic extension of nanometers long MWCNTs was realized with ultralow friction.¹⁹ As a recent breakthrough, we experimentally demonstrated that centimeters long inner walls could be continuously pulled out from defect-free double-walled carbon nanotubes (DWCNTs) under ambient conditions, and the interwall friction was independent of the pull-out length.²⁹ In spite of the above progress, many key issues about the interwall friction and sliding behaviors in MWCNTs still remain unclear. For example, little is known about the influence caused by tube

Received: November 25, 2015

Revised: January 10, 2016

Published: January 19, 2016

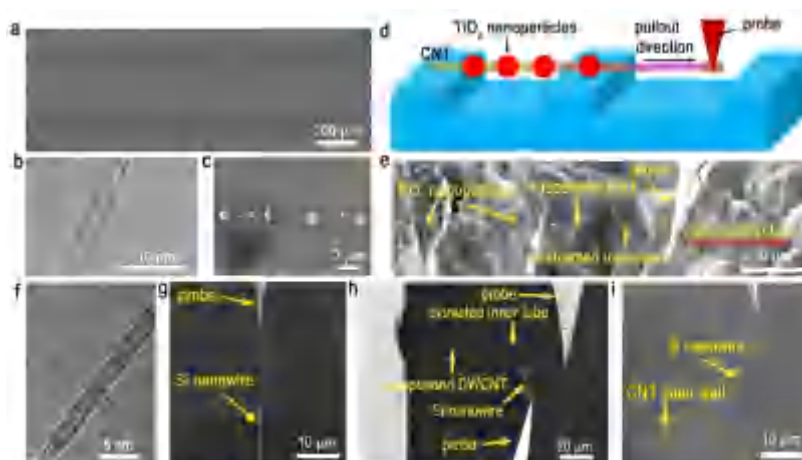


Figure 1. Pull-out of the inner wall from a DWCNT with a probe. (a) SEM image of as-grown ultralong CNT arrays. (b) High resolution TEM image of a DWCNT. (c) SEM image of a suspended DWCNT decorated with TiO_2 nanoparticles. (d) Illustration of pulling the inner wall out from a suspended DWCNT decorated with TiO_2 nanoparticles. (e) SEM image of pulling the inner wall out from a DWCNT (the z-direction of the probe movement is perpendicular to the plane). (f) TEM image of a DWCNT with inner wall partly pulled out. (g) SEM image of a silicon nanowire fixed on a tungsten probe. (h) SEM image of transferring the extracted inner wall from a probe to a silicon nanowire. (i) SEM image of using a silicon nanowire to measure the interwall friction of a DWCNT.

axial curvature and pullout velocity of inner walls on the interwall friction and sliding behaviors of MWCNTs. In addition, few experimental observations have been obtained on the effect of fractured ends on the interwall friction of MWCNTs. It is also of significance to investigate the issues such as the detailed inner wall sliding behaviors, the diameter variation, and the sequentially pull-out of different inner walls from MWCNTs, etc. Addressing these issues is essential to obtain a thorough understanding of the interwall friction and sliding behaviors in MWCNTs. In this work, we choose centimeters long DWCNTs as a prototype to investigate the interwall friction and sliding behaviors of MWCNTs. We find that the interwall friction shows a linear dependence of the pullout velocity of the inner wall. The interwall friction in curved DWCNTs is much higher than that of straight DWCNTs. The axial curvature plays a key role in the interwall friction of DWCNTs and also affects the sliding behaviors of the inner wall. Compared with the axial curvature, the opening ends of DWCNTs have weak influence on their interwall friction.

Horizontally aligned ultralong CNTs (Figure 1a) were synthesized on silicon substrates through chemical vapor deposition. DWCNTs with perfect structures (Figure 1b) were chosen for the interwall friction test. To facilitate the manipulation of individual DWCNTs, centimeters long silicon slices with trenches (0.1–1 mm wide, 5–10 mm long, and 0.1–0.5 mm deep) were used as substrates to grow DWCNTs in situ, which would partly suspend on the trenches (see Figure S1 in Supporting Information).^{30,31} Because of the nanometer-scale diameters of these DWCNTs, it is difficult to quickly find individual suspended DWCNTs in a scanning electron microscope (SEM) even with high resolution. To quickly identify the position and orientation of individual suspended DWCNTs, we decorated them with TiO_2 nanoparticles, which were proven to be a good indicator to show the position of individual suspended DWCNTs even with low resolution (Figures 1c and S2).^{29–31} The TiO_2 nanoparticles only attached on the outer surface of the DWCNTs and had no influence on the pristine properties and interwall interactions of these DWCNTs.³⁰ To investigate the inner wall sliding

behaviors and the interwall interactions of DWCNTs, a tungsten probe was used to pull out the inner walls from DWCNTs (Figure 1d,e). The probe was fixed on a nano-manipulation stage fixed in a SEM (Figure S3). A suspended DWCNT was fixed onto the probe by depositing some amorphous carbon onto the contact point between them (Figure S4). After the deposition of amorphous carbon, the suspended DWCNT was able to be stretched by the probe. The TiO_2 nanoparticles deposited on the outer surface of the suspended DWCNTs were key to indicate the inner wall pull-out process. Figure 1, panel d is an illustration showing pulling the inner wall out from a DWCNT by a probe. As shown in Figures 1, panel e, and S5, when moving the probe from the left to the right, a suspended DWCNT was elongated and all the TiO_2 nanoparticles moved and changed their positions accordingly. With the continuous moving of the probe, a TiO_2 nanoparticle (shown by the red arrow in Figure S5) suddenly stopped moving but still kept in a line with all the other particles, indicating the outer wall of the DWCNT had been broken and began to remain in a free state. With the continuous moving of the probe, the inner wall was continuously pulled out from a DWCNT (Figure 1f). In addition, the extracted inner wall could also be transferred using the probe to a transmission electron microscopy (TEM) grid for the high resolution TEM characterization (Figure S6). To measure the interwall friction of the DWCNTs, silicon nanowires (30–40 μm in length, 100–250 nm in diameter) were employed as the force cantilevers (force constant: $K = 1\text{--}10\text{ nN}/\mu\text{m}$). Figure 1, panel g shows a silicon nanowire, which was fixed onto a tungsten probe by depositing amorphous carbon on the contact point between them.

As mentioned earlier, a probe was employed to stretch the suspended DWCNT, break its outer wall, and then pull the inner wall out. To measure the interwall friction of the DWCNT, as shown in Figure 1, panel h, once the inner wall was partly extracted by a probe, the partly extracted inner wall was carefully released from the probe and then directly attached to the silicon nanowire. The reason why we did not use the silicon nanowire alone to break the out wall of DWCNTs, pull the inner wall out, and then directly measure the interwall

friction lies in the following fact. As is known, the tensile strength of a CNT wall is 50–120 GPa^{23,31,32} depending on the defects in the CNTs. For a DWCNT with the outer diameter of 3 nm, the total force needed for breaking its outer wall would be 350–850 nN, which is much larger than the interwall friction of the DWCNTs (usually 1–20 nN).²⁹ If we directly use the silicon nanowire to stretch the DWCNTs, there will be a large snap back of the soft silicon nanowire just after the DWCNT breaks, which will cause the sudden breaking of the inner wall and the total separation of the fragments. In comparison, the strategy proposed here, that is, transferring the partly extracted inner wall from the rigid tungsten probe to the soft silicon nanowire, offers an ideal method to smoothly pull out the inner walls from DWCNTs and measure their interwall friction. During the pulling-out of the inner wall from a DWCNT, the silicon nanowire had an axial deformation due to the tensile force caused by the interwall friction of the DWCNT (Figure 1i). The deformation of the silicon nanowire was recorded and the corresponding pulling force was obtained by multiplying the deformation of the silicon nanowire with its force constant K . According to Newton's Third Law of Motion, the interwall friction is equal to the pulling force.

In our previous work, we have measured the interwall friction of centimeters long straight DWCNTs with perfect structures, which are usually 1–4 nN, depending on the diameter of the DWCNTs.²⁹ However, many key issues about the interwall friction, such as the effects from the pullout velocity, the axial curvature, and the CNT ends, etc., still remain unclear. Here, we first investigated the relationship between the interwall friction and the pull-out velocity of the inner walls in DWCNTs. At the macroscale, dynamic friction is almost independent of the velocity. In contrast, friction force at the nanoscale exhibits obvious different behaviors, and numerous phenomena of velocity-dependence of friction were found on the nanoscale.^{26,33–38} A linear dependence of friction on velocity in simulations of oscillating CNTs was observed based on the assumption that the time scale for relative motion of the CNTs is large compared to the motion of the atoms within a given CNT.³⁹ Figure 2 shows the relationship of the pull-out

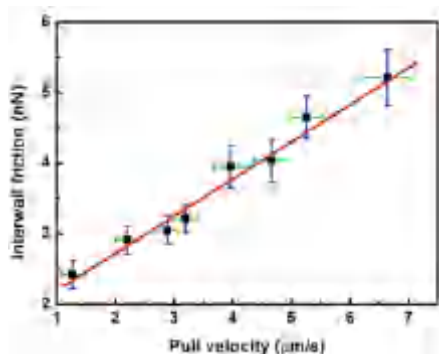


Figure 2. Relationship between the interwall friction and the pull velocity of inner wall.

velocity of the probe with the corresponding interwall friction of a 3 mm long DWCNT with diameter of 2.67 nm (Figure S7). The velocity was controlled by changing the speed of the rotation movement of the W-tip on the four-nanoprobe-system (see Methods). From the video taken on the SEM, we could directly get the pull velocity of the inner wall. The friction could be calculated from the deformation of the silicon nanowire.

From Figure 2, we can see that the larger the pull velocity is, the higher the interwall friction is, exhibiting a linear relationship with the pull velocity. This is the first experimental observation of the velocity-dependent interwall friction in CNTs. Molecular dynamics simulations were used to study the mechanical dissipation in nanometers long CNT oscillators, and the interwall friction in these CNTs was found to depend on the relative velocity of the inner walls.²⁵ This kind of velocity-dependent friction was believed to be a Stokes-like viscous drag.⁴⁰

The axial curvature has significant effect on the interwall interaction of DWCNTs. We use the curvature radius r (see Figure S8) to describe the axial curvature of a DWCNT. The smaller the curvature radius of a tube is, the higher the axial curvature. Figure 3, panel a shows the experimentally measured relationship between the interwall friction of DWCNTs and the axial curvature radius. The pullout velocity was kept to be 1 $\mu\text{m/s}$ during the whole experimental process. It is obvious that the interwall friction with higher curvature (i.e., smaller curvature radius) is higher than that with lower curvature. With the decrease of the curvature radius (i.e., the increase of the axial curvature), the interwall friction of the DWCNTs will increase accordingly. Especially, when the curvature radius of DWCNTs is smaller than 2 μm , the interwall friction have a sharp increase. For a DWCNT with a high axial curvature, there will be a large deformation energy in the curved DWCNT walls. Thus, the shear strength and the dissipation energy during the inner wall pull-out process will be much higher than that of straight DWCNTs, which accordingly causes a sharp increase of the interwall friction.

To further understand the effect of axial curvature on the interwall friction of DWCNTs, theoretical calculations were performed with a DWCNT with chiral index of (6, 6) @ (11, 11) chosen as a prototype to investigate the change of the wall–wall interaction in DWCNTs with axial curvatures. As shown in Figure 3, panel b, an axial curvature was exerted on a 50 nm long DWCNT. The persistence length of a CNT is about 0.8 μm ,⁴¹ which means that for a CNT with length shorter than 0.8 μm , we cannot treat it as a flexible or soft string but as a rigid rod. Therefore, when the DWCNT shown in Figure 3, panel b has an axial curvature, its wall–wall distances on the curved section will vary accordingly (Figure 3c). Besides, by using Figure 3, panel b, we can estimate the curvature radii corresponding to curvature height 1 and 5 nm to be about 0.35 and 0.07 μm , respectively. The dynamical friction force for the DWNT with these curvature radii should be at least 30–300-times greater than for straight DWNT. Here, we used the curvature height (Δh , shown in Figure 3b) to simply describe the degree of the axial curvature of the DWCNT. The higher the Δh , the larger the axial curvature. For the DWCNT of (6, 6) @ (11, 11), the equilibrium distance between both the top and the bottom walls is 3.365 Å. With the increase of the curvature height (Δh) from 0 to 50 Å, both the top wall–wall distance and the bottom wall–wall distance will break its equilibrium state, but exhibit different behaviors, separately. As shown in Figure 3, panel d, the top wall–wall distance (d_B) has a continuous decrease with the increase of Δh . When the Δh reaches 50 Å, the top wall–wall distance will be as low as 3.295 Å. In comparison, for the bottom wall–wall distance (d_T), it first increases until reaching a maximum value of 3.388 Å. After that, the bottom wall–wall distance decreases gradually and finally reaches 3.36 Å. The change of the wall–wall distances produced by the curved DWNTs breaks the equilibrium that

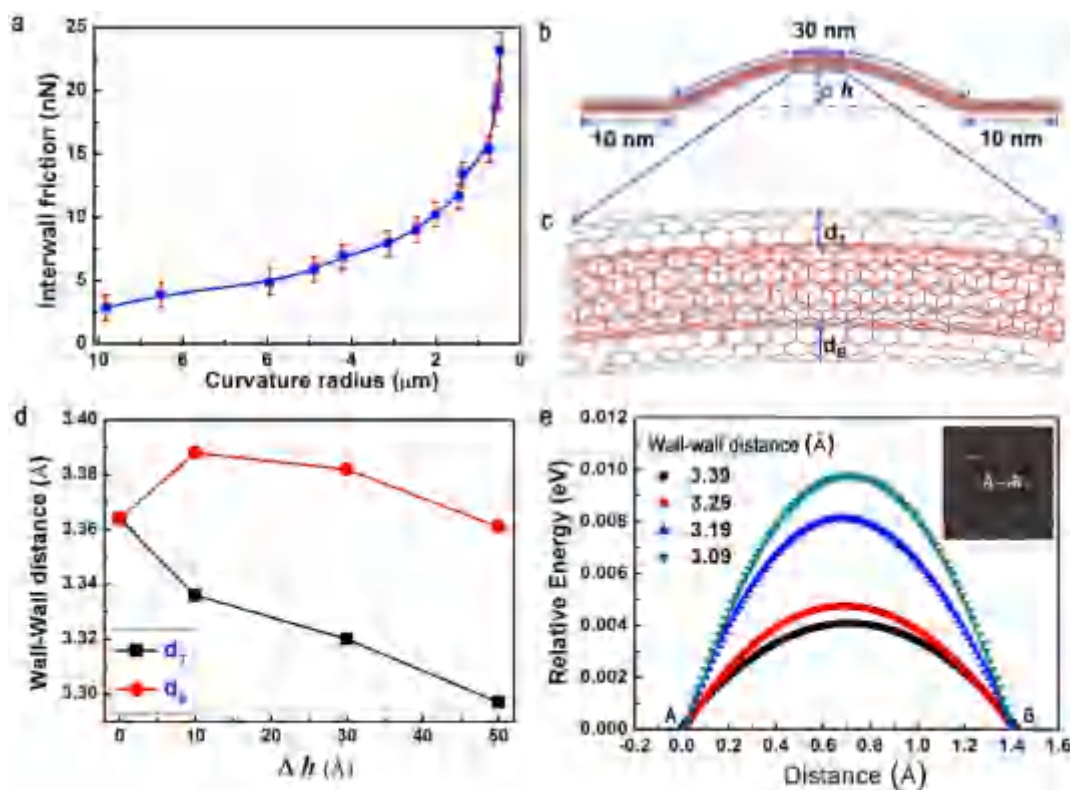


Figure 3. Effect on axial curvature on the interwall friction of DWCNTs. (a) Experimental relationship between the interwall friction and the axial curvature radius of DWCNTs. (b) Model of the curved DWCNT (6, 6) @ (11, 11) via lifting the middle section. Δh is the curvature height. (c) Enlarged illustration of the wall–wall distances of d_T and d_B in the rectangular box. (d) Relationship of wall–wall distance with curvature height. The definition of curvature height (Δh) is illustrated in panel b. (e) The variation of the relative vdW energy versus the sliding distance of a bilayer graphene (from A to B as shown in the inset) for different wall–wall distances. The sliding distance here refers to the distance when moving the one of the graphite layer shown in the inset in panel e from A to B.

exists in straight ones and causes a sharp increase of the relative potential energy between tube walls. As shown in Figure 3, panel e, the smaller the wall–wall distance, the higher the relative potential energy, that is, the larger the interwall friction. Thus, the axial curvature significantly affects the interwall interaction in DWCNTs. Similar results can also be obtained by using incommensurate bilayer graphene with smaller change of 0.06 Å to the wall–wall distance (see Figure S9).

The axial curvature also affects the sliding behavior of inner walls in DWCNTs. It is well-known that CNTs have a very high tensile strength but a relatively low shear strength.^{42,43} This makes the CNTs easily break under large shear deformation (i.e., with small bending angles). Figure 4 shows the breaking of both the outer and inner walls of a DWCNT under small bending angles. As shown in Figure 4, panels a and b, a probe was used to stretch a suspended DWCNT. The moving direction was initially vertical to the axial direction of the DWCNT. With the continuous moving of the probe, the outer wall of the DWCNT at the both sides broke, and then the inner wall was pulled out from the outer wall (Figure 4c). From Figure 4, panels c–g, we can see that the inner wall was continuously pulled out from the two broken ends of the original DWCNT. In the above process, the bending angle of the right section of the inner wall became smaller and smaller, while the bending angle of the left section first became smaller and then became larger (Figure 4d–h). When the bending angle of the right section of the inner wall reached 73°, the right section of the inner wall suddenly broke, while the left section of the inner wall still kept straight (Figure 4i). We can clearly

see that the outer wall (with TiO₂ nanoparticles as shown in Figure 4i) of the right section was also broken. As discussed earlier, the large axial curvature (i.e., small bending angles) results in the sharp increase of interwall friction, even the complete locking between the inner and outer walls, thus making the inner wall unable to be pulled out. With the continuous stretching of the DWCNT by the probe, the right section finally broke.

It has been reported, based on molecular dynamic simulation on the pullout of inner walls in MWCNTs, that inner walls with fractured ends have pullout forces 3–4-times larger than those for capped ends due to deformation of the fractured end.¹⁸ Besides, an ab initio study was conducted on the edge effect on relative motion of walls in carbon nanotubes.⁴⁴ It was reported that the ends provided a considerable contribution to the barrier to relative rotation of commensurate nonchiral walls. However, it is not clear about the end effect for the incommensurate CNTs. In addition, no experimental observation has been obtained yet. Here, we investigated the influence of open ends of inner walls on the interwall friction of DWCNTs. To get rid of the influence of root ends of ultralong DWCNTs on their interwall friction, we first cut them from the root ends by scratching them with a probe (shown in Figure 5a). The cutting off of a DWCNT was judged in the following way. When a voltage is exerted using the probe on a CNT, its color becomes dark in SEM. Once the CNT has been cut into two segments, only the one contacting the probe with a voltage becomes dark (Figure 5b,c). We measured the interwall friction of ultralong DWCNTs using the same method mentioned as

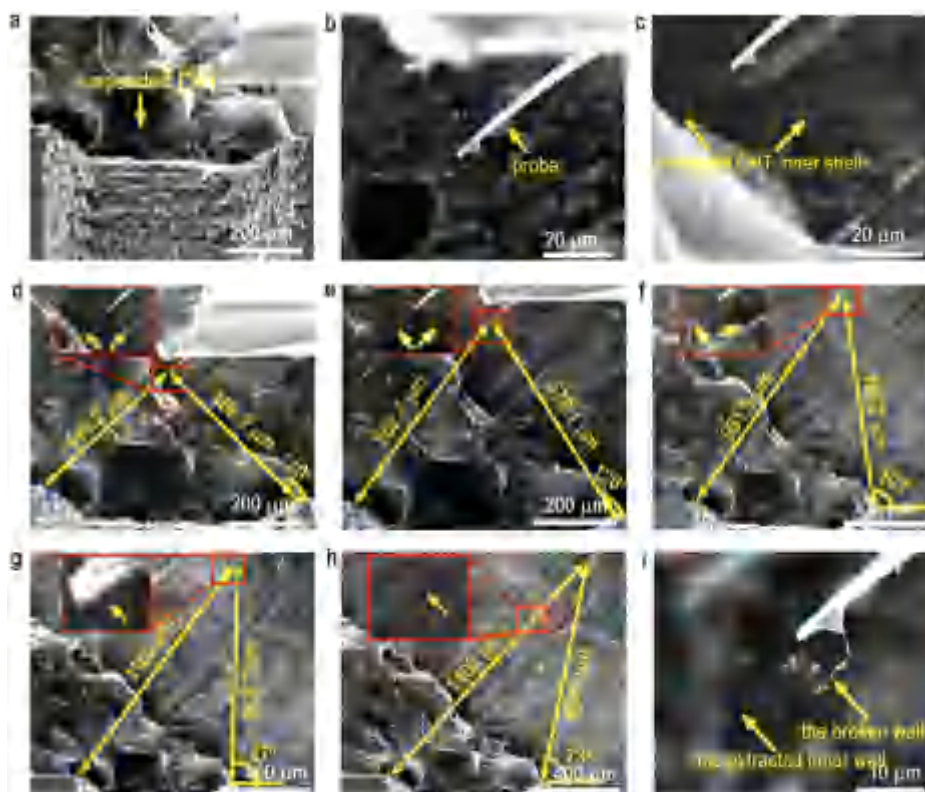


Figure 4. Influence of axial bending on the sliding behavior of inner walls. (a) There are two suspended DWCNTs across a trench on the substrate. (b) Stretching a suspended DWCNT with a probe. (c) The outer wall of the DWCNT broke, and the inner wall was pulled out from the outer wall. (d–g) The pulling out process of the inner wall at different bending angles. The insets are high resolution SEM images showing the extracted inner wall. (h, i) When the bending angle of the inner wall reached 73° , the right part of both the inner and the outer wall broke, while the left part still kept straight.

used previously. To investigate the effect of open ends on the interwall friction, we compared two different cases. As shown by Figure 5, panel d, the first case is cutting a DWCNT only once to make it get rid of the effect of root end. The second case is that cutting a DWCNT separately for many times, with pulling the inner wall out for a certain length for each time. Then we compared the forces needed for pulling the inner walls with cutting a DWCNT only once (single-cut) and cutting it many times (multicut). The pulling velocity of the inner walls in each DWCNTs was kept almost the same, about $1 \mu\text{m/s}$. The interwall friction of eight DWCNTs in the two different cases is shown in Figure 5, panel e. No obvious tendency can be seen. As was proven in our previous work,²⁹ for an ideal DWCNT with a partly pulled-out inner wall, the vdW interaction between the inner and outer walls can be divided into two sections: the overlapped section and the edge section. In the overlapped section, the interwall friction vanishes due to the repetitive breaking and reforming of vdW interaction between the adjacent walls. Theoretically, the total vdW interaction of a DWCNT only depends on the circumference of the outer shell (i.e., the edge section). Therefore, the interwall friction of a straight DWCNT with perfect structures is independent of overlap length of DWCNT walls. The fluctuation of the measured friction was mainly attributed to the axial curvature of the as-grown ultralong DWCNTs. Thus, compared with the axial curvature, the open ends have a weak effect on the interwall friction of DWCNTs.

In summary, we systematically investigated the interwall friction and sliding behaviors of centimeters long DWCNTs. A

special test system was established for the inner wall pulling out from the outer wall and the measurement of the interwall friction in DWCNTs. The interwall friction shows a linear dependence on the pullout velocity of the inner wall. The axial curvature of DWCNTs has a great effect on their interwall friction. Molecular dynamic simulation shows that the wall–wall distance varies greatly and causes a sharp increase of the relative wall–wall potential energy when a DWCNT has an axial curvature. This potential energy increase results in the interwall friction increase. The axial curvature also affects the sliding behavior of inner walls in DWCNTs. A large axial curvature (i.e., small bending angles) will result in the sharp increase of interwall friction, even the complete locking between the inner and outer walls, thus making the inner wall unable to be pulled out. This makes the CNTs easily break under large shear deformation. Finally, we compared the interwall friction of DWCNTs after cutting them single and multiple times and found that the opening ends of DWCNTs had no obvious effects on their interwall friction.

Methods. Substrate Preparation. Silicon substrate (5–10 mm wide, 10–100 mm long, and 0.5 mm thick) with 600 nm thick SiO_2 layer on the surface was used as the substrate for CNT synthesis. The silicon substrate was fabricated with many trenches (0.2–0.3 mm deep) across the whole substrate.

CNT Growth. The catalyst precursor used in this work was an ethanol solution containing FeCl_3 (0.04 mol L^{-1}), which was deposited onto the silicon substrate by microprinting method. The iron precursor became iron nanoparticles after reduction in H_2 and argon ($\text{H}_2/\text{Ar} = 2:1$ in volume with a total flow of 200

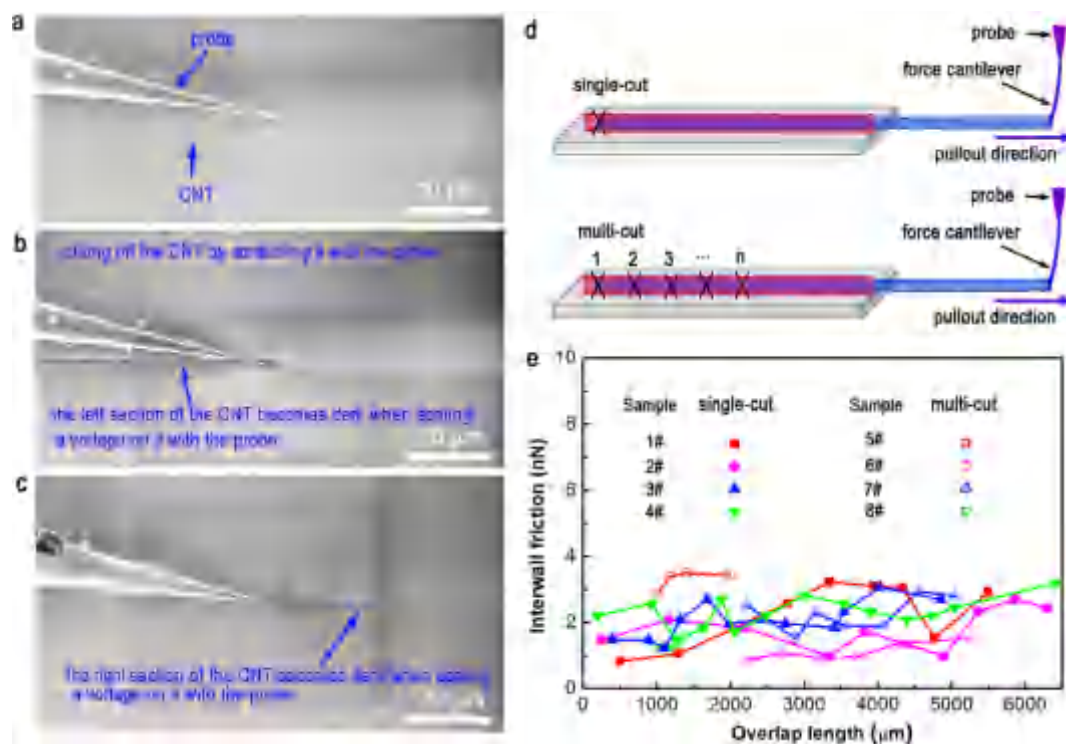


Figure 5. Effect of opening ends on the interwall friction of DWCNTs. (a) Moving a probe to a DWCNT on the substrate. (b) Cutting off the DWCNT by scratching with the probe on it. When applying a voltage through the probe onto the left section of the DWCNT, it became dark, but the right section still stayed bright. (c) When the right section of the DWCNT was in contact with the probe with a voltage, it became dark, while the left section became bright. (d) Illustration of cutting the DWCNTs for single or multiple times. (e) Comparison of friction of single-cut and multicut DWCNTs for different pull-out length.

sccm) at 900 °C for 25 min, which worked as catalysts for the growth of CNTs at 1000 °C. The carbon source was CH₄ mixed with H₂ (CH₄/H₂ = 1:2 in volume with a total flow of 75 sccm) together with 0.43% H₂O for accelerating CNT growth. The growth time for the CNTs was usually 10–20 min, which depended on the length of CNTs desired.

Deposition of TiO₂ Nanoparticles on CNTs. The substrates with suspended CNTs were taken into contact with TiCl₄ vapor in ambient conditions for depositing TiO₂ nanoparticles in a fume hood, where there was a humidity controller. The contact time usually ranged from 3.0–7.0 s. After that, there will be a lot of TiO₂ nanoparticles on the suspended CNTs.

Manipulation of Individual CNTs. A four-nanoprobe-system (MM3A nanoprobe, Kleindiek Company) inside a FEI XL30F SEM was used to manipulate individual CNTs. The nanoprobe arm with a W probe mounted on it can be moved in three directions: x, y, and z. The rotation movements in x- and y-directions enabled the arm to move on a surface of a sphere with an accuracy of about 2.5 nm. The radial movement of the W probe in z-direction has the finest step of 0.25 nm. The range of the rotation motor could be above 180°, while that of the radial motion is 12 mm. All three movements could be driven with varying speed. To measure the nanoscale forces of the interwall friction of CNTs, a silicon nanowire was mounted onto the W probe as a force cantilever. The force cantilever used here was a silicon nanowire (30–40 μm in length, 100–250 nm in diameter, force constant: K = 1–10 nN/μm, which was precisely measured using the electric field induced resonance method²⁸). The force cantilever was fixed onto the W probe attached on a nanoprobe arm. After the outer wall was broken and the inner wall was pulled out from a MWCNT, the

extracted inner wall was transferred from the probe to the force cantilever and fixed the inner wall onto the force cantilever by depositing some amorphous carbon on their contact point. Then, the inner wall could be continuously pulled out by moving the force cantilever to the right. The deformation of the force cantilever was recorded, and the corresponding pulling force could be obtained by multiply the deformation with K.

Cutting off a CNT with a Probe. First, cut off the CNT by scratching a probe on it. When the CNT was cut off, if a voltage was applied through the probe on one of the cutoff sections of the CNT, it would become dark, and the other section would still keep bright.

Characterization. The CNTs were characterized by SEM (JSM 7401F, 1.0 kV; FEI, XL30F, 3 kV), high-resolution TEM (JEM-2010, 120.0 kV), and Raman instrument (Horiba HR 800, 632.8 nm).

Theoretical Modeling and Calculation. The DWNT of (6,6) @ (11,11) in Figure 3, panel b is optimized by empirical potential including REBO² potential (describing carbon–carbon interaction of the intratube) and Lennard–Jones potential (describing the wall–wall interaction). To produce the curvature of the DWNT, the middle section of 30 nm length was lifted to the expected height generally (1 Å/lift) with the configure fully optimized for each lift. The relative vdW energies in Figures 3, panel e, and S5 for bilayer graphene are calculated by static calculation of the density functional theory (DFT).

Details of DFT Calculation. All the DFT calculations are performed by the Vienna Ab-initio Package (VASP). By using the Perdew–Burke–Ernzerhof (PBE), the generalized gradient approximation (GGA) is adopted for the exchange correlation

with the spin polarization taken into account. The plan wave cutoff energy is set to be 400 eV, and the projector-augmented wave (PAW) is used as the pseudopotential. The convergence criterion for energy and force is set to be 10^{-4} eV and 0.01 eV/Å, respectively. The unit cells for the commensurate and incommensurate bilayer graphene are $2.46 \text{ \AA} \times 4.26 \text{ \AA} \times 10$ and $8.67 \text{ \AA} \times 8.67 \text{ \AA} \times 10 \text{ \AA}$ with the Monkhorst–Pack k-point mesh of $14 \times 8 \times 2$ and $4 \times 4 \times 2$, respectively.

■ ASSOCIATED CONTENT

* Supporting Information

The Supporting Information is available free of charge on the ACS Publications website at DOI: [10.1021/acs.nanolett.5b04820](https://doi.org/10.1021/acs.nanolett.5b04820).

SEM image of ultralong CNTs grown on a silicon substrate with trenches on it; SEM image of suspended CNT decorated with TiO₂ nanoparticles; experimental setup for manipulating individual CNTs and measuring the interwall friction; SEM image of fixing a suspended CNT onto a tungsten probe by depositing a layer of amorphous carbon on the contact area; process of pulling out the inner wall from the DWCNT with a silicon nanowire; transferring the extracted inner wall with a probe to the TEM grid; TEM image of a DWCNT; illustration of curvature radius of a curved CNT; variation of the relative vdW energy versus the sliding distance of an incommensurate bilayer graphene for different wall–wall distances (PDF)

■ AUTHOR INFORMATION

Corresponding Authors

*E-mail: yingingzhang@tsinghua.edu.cn.

*E-mail: wf-dce@tsinghua.edu.cn.

Present Address

R.Z., Department of Materials Science and Engineering, Stanford University, Stanford, California 94305, United States.

Author Contributions

R.Z., Z.N., and Z.X. contributed equally to this work. The manuscript was written through contributions of all authors. All authors have given approval to the final version of the manuscript. R.Z., Y.Z., and F.W. proposed and conceived the project. R.Z. designed and performed the experiments and wrote the manuscript. R.Z. and Z.N. conducted the manipulation of CNTs in SEM. Z.X. and F.D. conducted the molecular dynamic simulation. Q.C., F.D., Q.Z., W.Q., and Y.C. participated in data analysis and the manuscript preparation. H.X. participated in the synthesis of ultralong CNTs.

Funding

The work is supported by the Foundation for the National Basic Research Program of China (2011CB932602, 2013CB934200), the National Science Foundation of China (51422204, 51372132, 11374022), and TNLIST Cross-discipline Foundation.

Notes

The authors declare no competing financial interest.

■ REFERENCES

- (1) Craighead, H. G. *Science* 2000, 290, 1532–1535.
- (2) Gnecco, E.; Bennewitz, R.; Gyalog, T.; Meyer, E. J. *Phys.: Condens. Matter* 2001, 13, R619–R641.
- (3) Urbakh, M.; Meyer, E. *Nat. Mater.* 2010, 9, 8–10.

- (4) Hirano, M.; Shinjo, K.; Kaneko, R.; Murata, Y. *Phys. Rev. Lett.* 1991, 67, 2642–2645.
- (5) Hirano, M.; Shinjo, K. *Phys. Rev. B: Condens. Matter Mater. Phys.* 1990, 41, 11837.
- (6) Verhoeven, G. S.; Dienwiebel, M.; Frenken, J. W. M. *Phys. Rev. B: Condens. Matter Mater. Phys.* 2004, 70, 165418.
- (7) Dienwiebel, M.; Pradeep, N.; Verhoeven, G. S.; Zandbergen, H. W.; Frenken, J. W. M. *Surf. Sci.* 2005, 576, 197–211.
- (8) Liu, Z.; Yang, J.; Grey, F.; Liu, J. Z.; Liu, Y.; Wang, Y.; Yang, Y.; Cheng, Y.; Zheng, Q. *Phys. Rev. Lett.* 2012, 108, 205503.
- (9) Hirano, M.; Shinjo, K.; Kaneko, R.; Murata, Y. *Phys. Rev. Lett.* 1997, 78, 1448–1451.
- (10) Gnecco, E.; Maier, S.; Meyer, E. J. *Phys.: Condens. Matter* 2008, 20, 354004.
- (11) Dienwiebel, M.; Verhoeven, G. S.; Pradeep, N.; Frenken, J. W. M.; Heimberg, J. A.; Zandbergen, H. W. *Phys. Rev. Lett.* 2004, 92, 126101.
- (12) Martin, J.; Donnet, C.; Le Mogne, T.; Epicier, T. *Phys. Rev. B: Condens. Matter Mater. Phys.* 1993, 48, 10583.
- (13) Guo, W.; Guo, Y.; Gao, H.; Zheng, Q.; Zhong, W. *Phys. Rev. Lett.* 2003, 91, 125501.
- (14) Zheng, Q.; Liu, J. Z.; Jiang, Q. *Phys. Rev. B: Condens. Matter Mater. Phys.* 2002, 65, 245409.
- (15) Li, Y.; Hu, N.; Yamamoto, G.; Wang, Z.; Hashida, T.; Asanuma, H.; Dong, C.; Okabe, T.; Arai, M.; Fukunaga, H. *Carbon* 2010, 48, 2934–2940.
- (16) Zheng, Q.; Jiang, Q. *Phys. Rev. Lett.* 2002, 88, 45503.
- (17) Yamamoto, G.; Liu, S.; Hu, N.; Hashida, T.; Liu, Y.; Yan, C.; Li, Y.; Cui, H.; Ning, H.; Wu, L. *Comput. Mater. Sci.* 2012, 60, 7–12.
- (18) Xia, Z.; Curtin, W. *Phys. Rev. B: Condens. Matter Mater. Phys.* 2004, 69, 233408.
- (19) Cumings, J.; Zettl, A. *Science* 2000, 289, 602–604.
- (20) Kis, A.; Jensen, K.; Aloni, S.; Mickelson, W.; Zettl, A. *Phys. Rev. Lett.* 2006, 97, 25501.
- (21) Fennimore, A.; Yuzvinsky, T.; Han, W. Q.; Fuhrer, M.; Cumings, J.; Zettl, A. *Nature* 2003, 424, 408–410.
- (22) Yu, M. F.; Yakobson, B. I.; Ruoff, R. S. *J. Phys. Chem. B* 2000, 104, 8764–8767.
- (23) Yu, M. F.; Lourie, O.; Dyer, M. J.; Moloni, K.; Kelly, T. F.; Ruoff, R. S. *Science* 2000, 287, 637–640.
- (24) Hong, B. H.; Small, J. P.; Purewal, M. S.; Mullokandov, A.; Sfeir, M. Y.; Wang, F.; Lee, J. Y.; Heinz, T. F.; Brus, L. E.; Kim, P.; Kim, K. S. *Proc. Natl. Acad. Sci. U. S. A.* 2005, 102, 14155–14158.
- (25) Tangney, P.; Louie, S. G.; Cohen, M. L. *Phys. Rev. Lett.* 2004, 93, 065503.
- (26) Tamba, N. S.; Bhushan, B. *Nanotechnology* 2005, 16, 2309.
- (27) Socoliuc, A.; Bennewitz, R.; Gnecco, E.; Meyer, E. *Phys. Rev. Lett.* 2004, 92, 134301.
- (28) Wei, X. L.; Liu, Y.; Chen, Q.; Wang, M. S.; Peng, L. M. *Adv. Funct. Mater.* 2008, 18, 1555–1562.
- (29) Zhang, R.; Ning, Z.; Zhang, Y.; Zheng, Q.; Chen, Q.; Xie, H.; Zhang, Q.; Qian, W.; Wei, F. *Nat. Nanotechnol.* 2013, 8, 912–916.
- (30) Zhang, R.; Zhang, Y.; Zhang, Q.; Xie, H.; Wang, H.; Nie, J.; Wen, Q.; Wei, F. *Nat. Commun.* 2013, 4, 1727.
- (31) Zhang, R.; Wen, Q.; Qian, W.; Su, D. S.; Zhang, Q.; Wei, F. *Adv. Mater.* 2011, 23, 3387–3391.
- (32) Yu, M. F.; Files, B. S.; Arepalli, S.; Ruoff, R. S. *Phys. Rev. Lett.* 2000, 84, 5552–5555.
- (33) Servantie, J.; Gaspard, P. *Phys. Rev. Lett.* 2006, 97, 186106.
- (34) Sang, Y.; Dubé, M.; Grant, M. *Phys. Rev. E* 2008, 77, 036123.
- (35) Krim, J. *Adv. Phys.* 2012, 61, 155–323.
- (36) Gnecco, E.; Bennewitz, R.; Gyalog, T.; Meyer, E. J. *Phys.: Condens. Matter* 2001, 13, R619.
- (37) Fusco, C.; Fasolino, A. *Phys. Rev. B: Condens. Matter Mater. Phys.* 2005, 71, 045413.
- (38) Evstigneev, M.; Reimann, P. Velocity dependence of atomic friction: Rate theory and beyond. In *Fundamentals of Friction and Wear*; Springer, 2007; pp 117–142.

- (39) Servantie, J.; Gaspard, P. *Phys. Rev. B: Condens. Matter Mater. Phys.* 2006, 73, 125428.
- (40) Muser, M. H. *Phys. Rev. Lett.* 2002, 89, 224301.
- (41) Sano, M.; Kamino, A.; Okamura, J.; Shinkai, S. *Science* 2001, 293, 1299–1301.
- (42) Ruoff, R. S.; Lorents, D. C. *Carbon* 1995, 33, 925–930.
- (43) Salvétat, J. P.; Bonard, J. M.; Thomson, N.; Kulik, A.; Forro, L.; Benoit, W.; Zuppiroli, L. *Appl. Phys. A: Mater. Sci. Process.* 1999, 69, 255–260.
- (44) Popov, A. M.; Lebedeva, I. V.; Knizhnik, A. A.; Lozovik, Y. E.; Potapkin, B. V. *J. Chem. Phys.* 2013, 138, 024703.